Geoderma 406 (2022) 115500

Contents lists available at ScienceDirect

Geoderma

journal homepage: www.elsevier.com/locate/geoderma

Phosphorus abundance and speciation in acid forest Podzols – Effect of postglacial weathering

J.R. Marius Tuyishime [a,*], Gbotemi A. Adediran [a], Bengt A. Olsson [b], Marie Spohn [a], Stephen Hillier [a,e], Wantana Klysubun [c], Jon Petter Gustafsson [a,d]

[a] Department of Soil and Environment, Swedish University of Agricultural Sciences, P.O. Box 7014, SE-75007 Uppsala, Sweden
[b] Department of Ecology, Swedish University of Agricultural Sciences, P.O. Box 7044, SE- 75007 Uppsala, Sweden
[c] Synchrotron Light Research Institute (SLRI), 111 Moo 6 University Avenue, Muang District, Nakhon Ratchasima 30000, Thailand
[d] Department of Sustainable Development, Environmental Science and Engineering, KTH Royal Institute of Technology, Teknikringen 10B, 100 44 Stockholm, Sweden
[e] The James Hutton Institute, Craigiebuckler, Aberdeen AB15 8QH, United Kingdom

ARTICLE INFO

Handling Editor: Andrew Margenot

Keywords:
P speciation
P stocks
Apatite weathering
Podzolization
P *K*-edge XANES spectroscopy

ABSTRACT

The molecular speciation of phosphorus (P) in forest soils is of strategic importance for sustainable forest management. However, only limited information exists about soil P speciation in boreal forests. We combined P *K*-edge XANES spectroscopy, wet chemical P extractions, and X-ray diffraction analysis of soil minerals to investigate the vertical distribution of P species in seven podzolised forest soils differing in soil properties and climatic conditions. The results showed that the total P stock was on average, 4.0 g m^{-2} in the Oe horizon, 9.5 g m^{-2} in the A and E horizons, and substantially higher (117.5 g m^{-2}, and 109.3 g m^{-2}) in the B and C horizons down to 80 cm depth, respectively. Although the Oe horizons contain a minor total P stock, 87% of it was stored as organic P. The composition of P species in the P-depleted A/E horizons was highly variable depending on the site. However, of the P stored in B and C horizons down to 80 cm, 58% was adsorbed P, mostly to Al, while apatite accounted for 25% of P, most of which was found in the C horizons. The apatite stocks in the A/E, B, and C horizons (down to 80 cm) accounted for 2.5%, 20%, and 77.2%, respectively, of the total apatite for all the mineral soils studied. These figures can be explained, first, by the dissolution of primary mineral apatite caused mainly by acidification. Second, P uptake by plants and microorganisms, and the associated formation of the Oe horizons, led to the formation of soil organic P. Further, the formation of organo-metal complexes and podzolization led to the translocation of P to the B horizons, where P accumulated mostly as P adsorbed to imogolite-type materials (e.g. allophane) and ferrihydrite, as shown by P *K*-edge XANES spectroscopy. In conclusion, this study shows that despite the young age of these soils (<15,000 years), most of the primary mineral apatite in the upper 30 cm has been transformed into organic P, and Fe-, Al-bound PO_4. Moreover, the subsoil P, mainly consisting of adsorbed P to Al, and apatite, dominates the P inventory and probably serves as a long-term buffer of P.

1. Introduction

Phosphorus (P) is an essential macronutrient whose availability in soil might constrain forest productivity, succession, and functioning (Elser et al., 2007, Jonard et al., 2015, Lang et al., 2017, Talkner et al., 2015, Vitousek et al., 2010). The total P stock and chemical speciation change with ecosystem development (Walker and Syers, 1976), which affects P availability. Phosphates (PO_4), which initially exist within poorly soluble primary minerals, become increasingly retained by newly formed secondary minerals (Walker and Syers, 1976).

Unlike nitrogen (N) that can be biologically fixed from the atmosphere, the atmospheric input of P in soils is small (Chadwick et al., 1999). The vast majority of P in soils is initially bound within primary Ca phosphate minerals (mostly apatite) (Nezat et al., 2007; Nezat et al., 2008; Prietzel et al., 2013). Apatite is progressively weathered, especially early during pedogenesis when the weathering rate is highest (Walker and Syers, 1976; Zhou et al., 2018). Thus, pedogenic apatite declines over geological time scales (Mehmood et al., 2018, Selmants

* Corresponding author.
E-mail address: marius.tuyishime@slu.se (J.R.M. Tuyishime).

https://doi.org/10.1016/j.geoderma.2021.115500
Received 4 December 2020; Received in revised form 9 August 2021; Accepted 18 September 2021
Available online 2 October 2021

and Hart, 2010), and the released P becomes biogeochemically active. In boreal and temperate coniferous ecosystems, organic matter-rich surface horizons form where decomposition and plant uptake are closely coupled (Wood et al., 1984). The fate of P in these soils is also affected by podzolization. Most Swedish forest soils were developed from glacially deposited, nutrient-poor parent material (Andersson et al., 2014). In these young boreal systems, the release of organic acids from the surface horizon and plant roots triggers silicate weathering, which leads to the formation of an illuvial E horizon (Lundström et al. 2000; Smits et al. 2014). Then, organic-acid-Al/Fe complexes migrate to the B horizon, where they precipitate mainly as imogolite-type minerals (ITM) (allophane/imogolite), but also as iron(III) (hydr)oxides (ferrihydrite and goethite) (Buurman and van Reeuwijk, 1984; Gustafsson et al., 1995; Gustafsson et al., 1999; Karltun et al., 2000; Lundström et al., 2000). These mineral phases have a very high P sorption capacity (e.g., Hewitt et al., 2021, Takamoto et al., 2021). Consequently, with time a large part of the biogeochemically active P may end up as adsorbed P in the B horizon (Adediran et al., 2020, Prietzel et al., 2016, Wood et al., 1984).

According to the model developed by Walker and Syers (1976), the total P stock decreases with time due to P leaching (Lang et al. 2016; Walker and Syers, 1976) unless tectonic uplift is strong enough to constantly provide substantial input of P from P-bearing minerals to the ecosystems (Buendia et al., 2010; Porder and Hilley, 2011). At a later stage of pedogenesis, the bioavailability of P is decreased, and P occluded within Al and Fe oxides and P associated with organic matter (OM) are the main pools of P (Turner and Condron, 2013; Walker and Syers, 1976). However, it has been argued that some forest soils in central and northern Europe, although at an early stage of soil development, are characterized by a low P nutritional status and P-limited conditions (Ilg et al., 2009; Yu et al., 2018), which may be affected by a low P availability of the P adsorbed to Fe and Al phases in the subsoil. Further, a high N availability due to high atmospheric deposition rates, enhanced forest productivity and intensified use of forest resources may contribute to an increased plant P demand (Akselsson et al., 2008; Heuck et al., 2018; Jonard et al., 2015; Mohren et al., 1986; Yanai, 1998). A mass balance study carried out for 14,550 Swedish sites showed that the annual losses of P from forestry exceeded 1 kg P ha^{-1} in Southern Sweden (Akselsson et al. 2008). Unless these losses are compensated for (i.e. by ash fertilization), the authors claimed that this may lead to a successive transition from N to P limitation.

To address questions relating to the P bioavailability and possible P limitation in the future, it is important to quantify the stocks of the different P species present in the soil. However, with the exception of a few studies on the P chemistry in the uppermost soil horizons (e.g., Giesler et al. 2002; Vincent et al. 2013), there are very few examples of research on P speciation in boreal forest soils detailed enough to provide reliable information on pedogenic P transformations and nutrient limitation. Synchrotron-based X-ray absorption near-edge structure (XANES) spectroscopy at the P *K*-edge is an emerging method, which provides a "fingerprint" for P speciation in soil (Beauchemin et al., 2003; Franke and Hormes, 1995; Hesterberg et al., 1999; Hesterberg, 2010). The spectra of different P species vary in one or more spectral features such as the shape and position of the white-line intensity as well as in post-edge and pre-edge structures (Beauchemin et al., 2003; Werner and Prietzel, 2015). However, P species coexist in a complex geochemical soil matrix, which makes it necessary to use careful and consistent interpretation methods to correctly separate different P species with P *K*-edge XANES spectroscopy (Gustafsson et al., 2020; Hesterberg, 2019). Important sources of uncertainty of XANES include the procedures of energy calibration at the beamline, and the choice of normalization parameters for linear combination fitting (LCF) (Colocho Hurtarte et al., 2019, Werner and Prietzel, 2015). However, as shown by Gustafsson et al. (2020), by careful energy calibration at the beamline, and by applying a probabilistic LCF method, these uncertainties can be minimized.

In this work, we combined bulk P *K*-edge XANES spectroscopy, wet chemical P extractions, and X-ray powder diffraction (XRPD) to investigate the P speciation of seven forest soils representing different soil properties and climatic conditions. The aim was to determine the stocks of the different P species that have developed after 8000–15,000 years of soil formation, particularly addressing the following questions: 1) what are the predominant P species in acid forest soils of Sweden? 2) does P speciation reflect weathering and podzolization in the soils? Our work builds on and extends the work of Adediran et al. (2020), who presented P speciation data for two of the soils of the current study (Tärnsjö and Tönnersjöheden). By analyzing a wider selection of soils, and by calculating the stocks of the different P species, this paper presents a more complete picture of the quantity of different P species and their vertical distribution in boreal forest soils.

2. Materials and methods

2.1. Study forest sites and soils

Soil phosphorus speciation was investigated in seven forest sites across Sweden that are located along a climate gradient ranging from 56 to 64°N (Fig. 1). They also encompass a variation in geochemical conditions and parent materials (Tables 1, 2, and S1). The sites are located on siliceous glacial till and in glaciofluvial or postglacial sandy deposits. The vegetation is dominated by Norway spruce (*Picea abies* L. Karst.) and Scots pine (*Pinus sylvestris* L.), and the soils are well-drained. These forest sites have previously been investigated for different purposes (Albaugh et al., 2009; Bergh et al., 1999; Casetou-Gustafson et al., 2019; Lim et al., 2020; Linder, 1995; Simonsson et al., 2015; Tiberg et al., 2018; Zetterberg et al., 2013). Five of them, Flakaliden 14B, 1470 Rödålund (North), Tärnsjö, Kloten (central) and Skogaby (SW) were classified as Albic

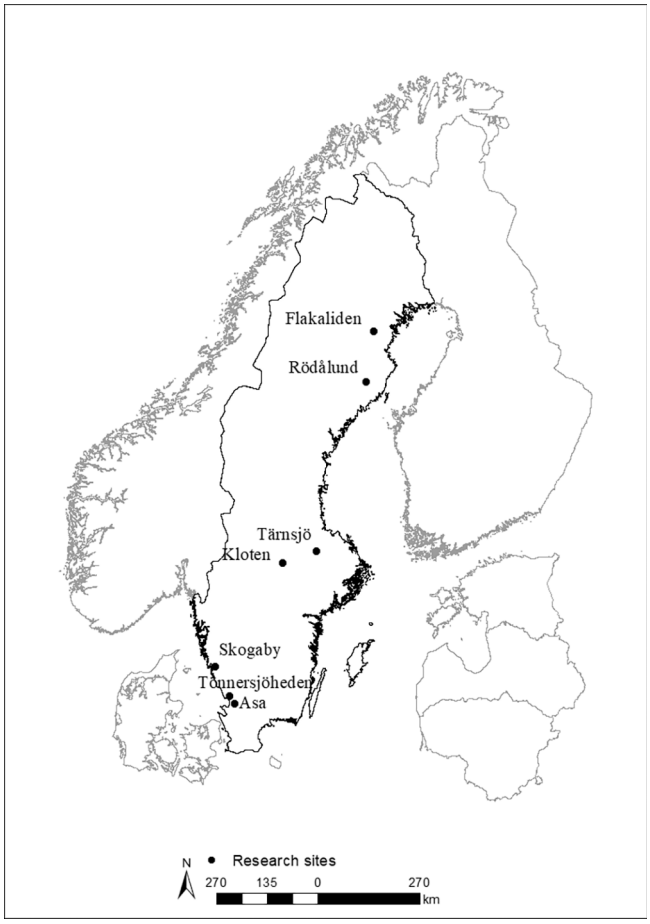

Fig. 1. Location of the study sites.

Table 1
Overview of the studied sites and soils organized by location. MAT is the mean annual temperature, and MAP is the mean annual precipitation.

Study site	Dominant tree species	Location	Parent rock	Soil order[a]	Altitude (m.a.s.l)	MAP mm	MAT °C
Flakaliden 14B	Norway spruce	64°07′N 19°27′E	Glacial till	Albic Podzol	315	600	1
1470 Rödålund	Scots pine	64°08′N 19°52′E	Wave-washed sand	Albic Podzol	250	600	2
Tärnsjö	Norway spruce Scots pine	60°08′N 16°55′E	Wave-washed sand	Albic Podzol	60	600	5.1
Kloten	Norway spruce Scots pine	59°54′N 15°25′E	Glacial till	Albic Podzol	345	927	4.9
Skogaby	Norway spruce	56°33′N 13°13′E	Glacial till	Albic Podzol	110	1187	7.6
Tönnersjöheden T103	Norway spruce	56°40′N 13°05′E	Glacial sandy till	Dystric Arenosol	80	1053	6.4
Asa	Norway spruce	57°08′N 14°45′E	Glacial till	Dystric Arenosol	240	800	6.4

[a] Soil classification according to IUSS Working Group WRB (2014).

Podzols (IUSS Working Group WRB, 2014). The Tönnersjöheden (T103) and Asa soils, both from SW Sweden, classify as Dystric Arenosols (IUSS Working Group WRB, 2014), although the former was very close to being an Entic Podzol. The reason why the Tönnersjöheden soil was not classified as a Podzol was that the A horizon had probably been mixed with large amounts with B horizon material so that the $Al_{ox}+½Fe_{ox}$ value (in g kg^{-1}) in the A horizon was slightly more than half of the $Al_{ox}+½Fe_{ox}$ value in the upper B horizon (Table S1). Also the Asa soil was very probably subject to podzolization in the past. The historical land use on this site with stone cairns, mechanical soil scarification (Casetou-Gustafson et al., 2020) might have caused soil mixing or overturn of the surface soil horizons.

2.2. Mineralogical characterization by X-ray powder diffraction (XRPD)

For all samples, sieved (<2 mm) samples were micronized in a McCrone mill, and random powders prepared by spray drying the resulting slurries (Hillier, 1999). XRPD patterns were recorded from 4 to 70°2θ using a Bruker D8 diffractometer with Cu K-α radiation and a Lynxeye XE position sensitive detector. Crystalline minerals were identified by aid of patterns from the International Center for Diffraction Data (ICDD) Powder Diffraction File (PDF-4, 2021) and using Bruker DiffracPlus EVA software. Quantitative mineralogical analysis of the diffraction data was performed using a pre-determined full pattern fitting approach as outlined by Omotoso et al. 2006 (participant 18), and more recently by Butler and Hillier (2021). The method does not require the addition of an internal standard but instead includes patterns for amorphous/poorly crystalline phases to enable their direct quantification. The mineralogical composition of bulk soil samples from the Skogaby site was studied previously by Simonsson et al. (2016), while that of the Asa and Flakaliden sites was determined by Casetou-Gustafson et al. (2018). Tönnersjöheden soil mineralogy analysis was carried out at the same time as Flakaliden and Asa but the data has not yet been published. Both previous studies used similar methods, but for the present study the Skogaby soils were rerun on the D8 diffractometer, and the Asa and Flakaliden XRPD data files run previously on the D8 retrieved so that all samples were fitted using precisely the same fitting parameters and full pattern library for the D8 diffractometer. This ensures internal consistency and enables the best comparison of mineralogical analyses from one sample to another.

The results (% by weight) show that the mineralogy of all seven studied soils was dominated by quartz, plagioclase, and potassium feldspar (Table S1). In the B horizon, the highest proportions of amorphous Fe and Al phases, which represent ferrihydrite and allophane were found in the Kloten and Flakaliden soils, which agrees with the wet chemical results, and which is evident also in the P speciation results, see below. In addition, apatite was detected by XRPD mainly in the subsoils except for the Kloten profile where no apatite was detected by XRPD.

2.3. Characterization of chemical soil properties

At each site, a soil pit was excavated and its profile was exposed and prepared for collecting samples (Fig. S3). In total, 73 samples were collected in 10 cm intervals, except for the Oe and E horizons, which were sampled by horizon. The sampling of the Oe and E horizons was adopted to be able to calculate the horizon-specific P stocks in the studied podzolized soils. The Oe horizon thickness ranged between 5 and 7 cm depending on the site. The samples were air-dried, at approximately 30 °C for 7 days and sieved (<2 mm) using a sieve with stainless steel mesh. The soil pH was measured in water using a soil: solution ratio of 1:2.5 (Van Reeuwijk, 1986) for mineral soil samples and a 1:10 ratio for the Oe samples (Blakemore, 1987) after 24 h equilibration time. The amount of organic carbon (C_{org}) and total nitrogen in the soil was determined through dry combustion according to ISO 13878 (1998), using an elemental analyzer for macrosamples (TruMac ® CN, Leco corp, S:t Joseph, MI, USA). Acid-digestible P (TP) was determined by microwave-assisted HNO_3/H_2O_2 digestion of 1 g dry soil according to the method of Church et al. (2017). While this is considered as total P, it should be noted that there may be a small proportion of the P in the soil matrix that is not solubilized by acid digestion procedures (ISO 11074:2015). Surface-reactive Al, Fe, Si and P associated with poorly crystalline Al and Fe minerals (Al_{ox}, Fe_{ox}, Si_{ox} and P_{ox}) were determined using oxalate extraction according to Van Reeuwijk (1986). Briefly, 100 mL acid ammonium oxalate solution (pH = 3.0) was added to 1 g dry soil in 250 mL polyethylene dark bottles covered by aluminium foil. The mixture was equilibrated for 4 h in the dark using an end-over-end shaker. Prior to analysis of Al_{ox}, Fe_{ox}, and Si_{ox} by ICP-OES (inductively coupled plasma optical emission spectroscopy) using a Thermo iCAP 6300 instrument (ThermoFisher Scientific, Waltham MA, USA), the extract was filtered through 0.2 μm single-use filters (Sartorius Minisart®) and diluted five times with ultra-pure H_2O. Further, molybdate-reactive P (Pi_{ox}), representing orthophosphate (Pi_{ox}) in the oxalate extract, was analysed separately using a Seal AA3 AutoAnalyzer (Seal Analytical, Norderstedt, Germany), using the acid molybdate method as modified by Wolf and Baker (1990). The difference between P_{ox} and Pi_{ox} was assigned to oxalate-extractable organic P ($P_{org\text{-}ox}$). Further, the degree of P saturation (DPS) on Al and Fe was calculated using the molar concentrations of Al and Fe bound P as determined by XANES:

$$DPS = \frac{XANES\text{ - }derived\ Al + Fe\text{ - }bound\ P}{0.5 \times (Fe_{ox} + Al_{ox})} \quad (1)$$

Pyrophosphate-extractable Al (Al_{py}) and Fe (Fe_{py}), representing Al and Fe bound to organic matter, were determined with ICP-OES after 1 g dry soil had been equilibrated in 100 mL of 0.1 M Na pyrophosphate for 16 h (Van Reeuwijk, 1986). Acid ammonium lactate (AL)-extractable P (P-AL), representing short-term geochemically active P, was determined after shaking 3 g of dry soil in 60 mL of AL buffer (adjusted to pH 3.75) for 1.5 h (Egnér et al., 1960) and subsequent analysis by ICP-OES. Plant-available P (P_{Ols}) was determined according to Olsen (1954). Briefly, 2 g soil was equilibrated for 0.5 h with a 40 mL solution containing 0.5 M $NaHCO_3$ (with pH adjusted to 8.5). The suspension was filtered (0.2 μm) before analysis using an AA500 AutoAnalyzer (SEAL analytical). The C_{org}: $P_{org\text{-}lcf}$ and N: $P_{org\text{-}lcf}$ P ratios were calculated based on mol kg^{-1} concentrations of C_{org} and total nitrogen (N) in the soil OM and XANES-derived organic P ($P_{org\text{-}lcf}$). For each soil horizon, the P stocks, i.e. the amount of TP, and P species in g m^{-2} for each soil depth was calculated according to Strand et al. (2016), as follows:

Table 2
Horizon-average properties of the studied soils (mean values).

Horizon	Depth cm	pH	TP	Al_{py}	Fe_{py}	Al_{ox}	Fe_{ox}	Si_{ox}	P_{ox}	Pi_{ox}	$P_{org\text{-}ox}$	P-AL	P_{Ols}	DPS	C	N	$C:P_{org*}$	$N:P_{org*}$	Al:Si
			mmol kg^{-1}											%	g kg^{-1}		mol mol^{-1}		
Flakaliden 14B																			
Oe	>0	4.1	18.3	9.9	5.4	18.3	10.8	0.2	9.1	4.2	4.9	6.6	2.9	14.0	208.0	6.0	1040.0	26.0	35.9
E	0–20	4.5	2.0	4.3	1.5	10.7	3.0	0.2	0.9	0.3	0.6	0.5	0.2	12.0	7.7	0.4	951.0	39.5	33.0
B	20–50	4.9	24.4	128.2	33.3	415.5	169.3	108.4	22.6	19.8	2.8	1.0	0.8	8.3	16.4	0.7	n.c	n.c	2.7
C	50–100	5.3	16.7	35.5	2.5	136.3	35.2	44.1	12.2	10.9	1.3	1.5	0.4	15.2	2.9	0.1	n.c	n.c	2.3
1470 Rödålund																			
Oe	>0	4.0	19.2	36.4	4.5	48.2	12.6	0.6	5.3	2.7	2.6	4.6	1.8	9.4	434.0	12.6	2213.0	55.0	18.8
E	0–20	4.5	1.7	12.0	4.8	18.7	12.8	1.2	1.2	0.5	0.7	0.2	0.1	3.6	3.8	0.2	356.0	11.0	7.0
B	20–50	5.4	5.6	57.7	7.3	153.2	25.4	48.6	2.9	2.2	0.7	0.1	0.1	4.3	4.5	0.2	301.0	9.0	1.9
C	50–80	5.4	12.1	35.8	4.1	127.5	25.2	42.2	8.0	7.0	1.0	1.3	0.2	11.9	2.4	0.1	227.0	8.0	2.2
Tärnsjö																			
Oe	>0	4.0	18.4	18.8	2.0	25.3	8.9	0.5	4.3	2.6	1.7	4.4	2.2	11.0	467.0	12.4	2314.0	53.0	13.4
E	0–2	4.3	2.0	4.6	2.5	10.4	4.2	0.4	0.5	0.2	0.4	0.2	0.1	0.0	8.0	0.2	n.c	n.c	13.1
B	2–40	5.0	15.5	46.5	12.5	104.3	39.6	20.9	11.6	10.2	1.5	1.3	0.8	19.8	7.0	0.2	1665.0	42.5	2.8
C	40–100	6.0	14.7	10.3	2.4	31.3	12.3	13.3	3.0	2.5	0.5	0.6	0.2	24.8	0.7	<LOD	n.c	n.c	1.5
Kloten																			
Oe	>0	3.9	18.3	23.5	5.7	31.4	14.5	0.7	4.8	2.5	2.3	5.0	2.2	7.0	438.0	13.4	2214.0	58.0	10.7
E	0–7	4.1	1.7	13.4	5.2	17.4	5.9	0.5	0.8	0.1	0.7	0.3	0.1	6.0	22.0	0.7	1896.0	50.0	8.4
B	7–40	5.0	9.2	238.9	76.1	576.1	185.1	140.8	6.5	4.1	2.4	0.2	0.1	1.8	29.8	1.1	717.3	23.3	2.4
C	40–50	5.2	7.3	48.4	5.2	176.3	34.7	57.2	5.6	4.4	1.2	0.2	0.1	6.0	4.0	0.2	n.c	n.c	2.2
Skogaby																			
Oe	>0	3.4	20.6	25.9	5.7	33.3	13.9	0.3	7.9	3.6	4.4	6.2	3.8	23.0	424.0	14.7	2340.0	69.0	26.7
E	0–10	3.6	4.1	28.5	39.3	27.0	38.8	1.1	3.4	1.0	2.4	1.1	0.6	9.5	37.1	1.5	2761.5	93.5	–
B	10–60	4.4	7.2	113.3	50.6	207.8	110.0	38.3	6.0	3.6	2.4	0.1	0.1	4.0	16.2	0.7	1084.3	38.5	2.4
C	60–100	4.7	8.3	26.7	3.0	47.6	5.5	12.0	3.8	3.0	0.8	0.7	0.1	14.0	1.6	<LOD	n.c	n.c	1.7
Tönnersjöheden (T103)																			
Oe	>0	3.7	21.6	19.2	7.2	26.2	13.8	0.6	5.5	2.1	3.3	4.8	2.2	15.0	448.0	14.7	1951.0	55.0	11.0
A	0–10	4.2	8.3	96.5	121.2	98.7	131.7	2.7	5.6	2.0	3.5	0.8	0.2	5.0	40.0	1.6	1679.0	59.0	0.9
B	10–50	4.7	16.9	141.9	43.7	260.6	82.5	49.6	12.5	9.1	3.5	0.6	0.3	8.3	18.3	0.9	662.3	27.3	2.4
C	50–100	4.8	14.6	63.8	16.0	90.7	24.8	17.1	7.6	5.7	1.9	0.9	0.1	13.6	6.4	0.2	n.c	n.c	1.5
Asa																			
A	0–10	4.5	11.8	191.5	74.7	205.1	82.2	22.3	7.6	3.3	4.3	0.9	0.3	4.0	53.6	2.5	2228.0	40.0	0.6
B	10–50	4.5	11.4	203.6	77.9	201.8	85.9	20.1	7.8	3.2	4.6	0.9	0.2	4.8	45.4	2.0	1123.0	19.0	0.3
C	50–100	4.6	15.3	92.0	21.4	92.0	32.9	27.8	9.2	7.2	2.0	1.7	0.1	10.4	9.3	0.4	1.0	n.c	1.8

P_{org}*: organic P as evidenced by XANES ($P_{org\text{-}lcf}$). Al:Si calculated as (Al_{ox} - Al_{py})/Si_{ox}. n.c: not calculated because Porg* was not detectable by XANES. < LOD: below the limit of detection. For more details of all samples, see Table S1.

$$P_{stock} = BD*CF_{coarse}*P*d \quad (2)$$

where BD represents bulk density (kg m^{-3}), CF_{coarse} is the correction factor for stones and boulder contents (=1-(stone volume %)/100), P is the P content (kg kg^{-1}), *d* is the sampling depth increment within the soil horizon (m). The CF_{coarse} was adopted from earlier studies (Asa and Flakaliden, Casetou-Gustafson et al. 2020; Rödålund, Lim et al., 2020; Tärnsjö, Kloten, and Skogaby, Stendahl et al. 2009) in which stoniness had been estimated by the rod penetration method (Stendahl et al., 2013; Viro, 1952), or had been estimated from pit excavations where the volume of stones and gravel was measured (Tönnersjöheden). However, some of the soils are shallow and so the P stocks were not calculated for the whole profile. BD was estimated from the organic C content using the pedotransfer functions developed by Nilsson and Lundin (2006):

$$BD\ mineral\ soil = 1000\cdot\left(1.5463\cdot e^{-0.3130\cdot\sqrt{C_{org}}} + 0.207\cdot d\right) \quad (3)$$

$$BD\ humus = 1000\cdot\left(\frac{C_{org}}{-2.1278 + 0.1528\cdot C_{org} + 0.2105\cdot C_{org}^2}\right) \quad (4)$$

where C is the organic carbon content (% dry weight).

2.4. Phosphorus speciation by X-ray absorption near-edge structure (XANES) spectroscopy

To investigate P speciation at the pedon scale, P *K*-edge XANES spectroscopy was performed on bulk samples of all Oe, A/E, B and C horizons (Fig. 3 and Table S1) at beamline 8 (BL 8) (Klysubun et al., 2020) of the Synchrotron Light Research Institute (SLRI) in Nakhon Ratchasima, Thailand. The BL8 utilizes synchrotron radiation generated from the SLRI storage ring with an electron beam energy of 1.3 GeV and a beam current ranging from 80 to 150 mA. The X-ray photon energy was scanned by an InSb (1 1 1) double crystal monochromator giving a beam flux of 1.3×10^9 to 3×10^{11} photons s^{-1} (100 mA)$^{-1}$ of 17.7×0.9 mm^2 beam. The soil samples were homogenized, finely ground and sieved (to <50 μm) to optimize X-ray beam penetration in the sample and to minimize the effect of self-absorption. The samples were packed in hollow and stainless steel sample holders (2 mm thick, 1×1.5 cm^2 with a sample window of 0.5×1 cm^2), which were covered with polypropylene X-ray film (Eriksson et al., 2016b). The sample holder was mounted in the sample compartment at 45^0 relative to the incident monochromatic beam. The sample compartment was continuously evacuated with helium (He) gas to lessen the attenuation of X-ray absorption (Kelly et al., 2008). A solid-state 13-element Ge detector measured the fluorescence emitted from the sample in the energy range of 2100–2320 eV. A 2 s dwell time was used per energy step. This energy step was 2 eV between 2100 and 2139 eV, 1 eV between 2139 and 2146 eV, 0.2 eV between 2146 and 2160 eV, 0.3 eV between 2160 and 2190 eV, and 5 eV between 2190 and 2322 eV. The maximum of the first derivative of the spectrum (E_0) for the black P was set to 2145.5 eV for energy calibration. A variscite standard (E_0 = 2154.05 eV) was frequently measured to check any shift that occurred after every energy re-calibration. Between 4 and 8 scans were collected for each sample.

2.4.1. P K-edge XANES data processing

The computer code Athena, Demeter version 0.9.025 (Ravel and Newville, 2005), was used for all XANES spectral data processing. Before merging multiple scans of a given sample, each scan was examined thoroughly for its quality (e.g. glitches, noise), and, if necessary, corrected for any misalignment of energy, as indicated by the variscite calibration check. The normalization of spectra was carried out as follows: first, correction of the linear baseline by subtracting a linear function from the spectral range below the edge at −30 and −10 eV relative to E_0 = 2154.05 eV (the first-derivative maximum of the P *K*-edge of variscite). Second, the post-edge normalization range was determined by a linear function between 30 and 45 eV relative to E_0 = 2154.05 eV, as a starting point (Eriksson et al., 2016b). Each normalized sample spectrum was thereafter subjected to linear combination fitting (LCF) analysis (Beauchemin et al., 2003). In the current study, 15 standards divided into six species groups were used to provide a good representation of the solid P phase in acid forest soil (Gustafsson et al., 2020):

1. *Soil organic P* (representing generic organic P from a Spodosol Oe horizon).
2. *Phosphate adsorbed to Al*: phosphate adsorbed to allophane, phosphate adsorbed to gibbsite, and phosphate adsorbed to $Al(OH)_3$
3. *Phosphate adsorbed to Fe*: phosphate adsorbed to ferrihydrite, phosphate adsorbed to goethite
4. *Al phosphates*: variscite, amorphous $AlPO_4$
5. *Fe (III) phosphates*: strengite, amorphous $FePO_4$
6. *Ca phosphates*: apatite Taiba, apatite Templeton, hydroxyapatite, octacalcium phosphate (OCP), brushite.

In the LCF, energy shifts were not permitted, the sum of weights (SOW) was not forced to 1, and a maximum of four standards was allowed in the output. The best fit was chosen from all the output fits, as resulted in the lowest R factor (goodness-of-fit parameter of Athena) (Ravel, 2009).

$$R = \frac{\sum(\text{data - fit})^2}{\sum(\text{data})^2} \quad (6)$$

Moreover, only LC fits having a SOW between 0.95 and 1.05 were accepted. The LC fits were then subject to uncertainty analysis with the AthenaAut software, as detailed by Gustafsson et al. (2020). Briefly, 100 spectral variants for each single LC fit were generated by Latin hypercube sampling. For misalignment in energy calibration and normalization errors, we used Beta (α, β) probability distributions with $\alpha = \beta = 1.5$. The maximum energy calibration error, which is equivalent to 0- and 100 percentiles was set to −0.05 eV and 0.05 eV, respectively. The maximum error in normalization was estimated to be 7% below and at E_0, which then decreased linearly to 0 at the lower post-edge normalization limit (set to +30 eV relative to E_0 = 2154.05 eV). Each of the 100 spectral variants was then subjected to LCF analysis and the best results for all LCF:s were retrieved. Only models that could describe at least 50% of spectral variants were accepted. To improve statistics for the spectra not covered at 50%, we grouped different species groups into larger groups following the procedure of Gustafsson et al. (2020). For example, all Fe-bound P (phosphate adsorbed to Fe and Fe phosphate) could be grouped into a single group termed “Fe-bound P” if this was necessary to reach 50 %. The concentrations of XANES-derived P species were calculated from the LCF-generated P fractional weights of the TP concentration (in 100%). The fit uncertainty associated with energy calibration and normalization errors was also calculated according to Gustafsson et al. (2020). In this study, the resulting uncertainties of the different fractions were generally in the order of 5 % of TP.

When presenting the results from LCF, we assumed that the sum of all weights corresponded to TP. However, the X-ray beam is not able to penetrate the soil particles more than a few μm at the P *K*-edge, as was discussed by Eriksson et al. (2016a), while the soil samples had been crushed and sieved to <50 μm. On the other hand, the assumption that acid-digestible P represents TP is similarly uncertain. Hence, the assignment of XANES-derived weights to percentages of TP may not be completely correct, but the weights should be reasonably accurate concerning the relative concentrations of geochemically active (i.e. surface-active) P species in the soil.

3. Results

3.1. Soil characteristics

The characteristics of the studied soils are presented in Table 2 (horizon-averaged data) and Table S1 (data for all individual samples). In all investigated profiles, the pH was low and increased slightly with depth. On average, the pH was 3.9, 4.2, 4.7 and 5.2 in the Oe, A/E, B and C horizons, respectively. The amounts of C_{org} and total N (N) were high in the Oe horizons and decreased substantially with soil depth. When using the XANES-derived organic P from LCF, $P_{org\text{-}lcf}$, the element ratios C_{org}: $P_{org\text{-}lcf}$ (mol mol^{-1}) ranged between 1040 and 2340 in the Oe horizons. In the mineral soil, these ratios increased generally from the North to the South and decreased with increasing soil depth. In the A/E horizons, the C_{org}: $P_{org\text{-}lcf}$ ratios were below 1000 for the two northern sites, Flakaliden and Rödålund, and between 1679 and 2762 for the remaining sites. The N: $P_{org\text{-}lcf}$ (mol mol^{-1}) ratio varied between 9 and 93.5 and appeared to be higher for the southern sites, when samples from the same depths are compared.

The concentrations of oxalate-extractable Al (Al_{ox}) and Fe (Fe_{ox}) peaked in the B horizons (the maximum concentrations for all samples were between 166.5 and 821.7 mmol kg^{-1} for $Al_{ox,}$ and between 64.2 and 366.9 mmol kg^{-1} for Fe_{ox}), see Fig. S1. In the C horizons, the concentrations ranged from 25.3 to 188.1 mmol kg^{-1} for Al_{ox} and from 3.9 to 41 mmol kg^{-1} for Fe_{ox}. Minimum concentrations were measured in the E horizons. The concentrations of pyrophosphate-extractable Al (Al_{py}) and Fe (Fe_{py}) were lower than Al_{ox} and Fe_{ox}. Two contrasting soils were those of Kloten and Tärnsjö, which had the greatest and lowest accumulation of both oxalate- and pyrophosphate-extractable Al and Fe, respectively. On a molar basis, the Al_{ox} concentration was always higher than Fe_{ox}, except in the A/E horizons of Tönnersjöheden and Skogaby. The data also revealed that the inorganic Al:Si ratio of the oxalate extract, calculated as (Al_{ox}-Al_{py})/Si_{ox}, was consistently between 2 and 3 in the B horizons (Table S1), suggesting ITM (i.e. allophane and imogolite) to be the dominant form of inorganic oxalate-extractable Al (Gustafsson et al., 1999; Gustafsson et al., 1995; Lundström et al., 2000). The DPS ranged between 1 and 34% with the highest and lowest percentages at Tärnsjö and Kloten, respectively. In the B horizons, the former site also showed a higher DPS level, being 2 to 10 times higher than that found in similar horizons at the other studied sites.

3.2. Contents of different extractable P fractions as assessed by wet chemical extractions

The acid-digestible P (TP) concentration ranged from 1.1 to 29.7 mmol kg^{-1} (median = 12.5 mmol kg^{-1}) across all analyzed 73 samples, of which between 13 and 98% could be dissolved in acid ammonium oxalate (Table 2, Table S1). Of the oxalate extractable-P (P_{ox}), on average 66% was Pi_{ox}, and the remaining part was assumed to represent organic P ($P_{org\text{-}ox}$) (Table 2). The extracted P increased in the order P_{Ols} < P-AL < P_{ox} < TP. Both TP and P_{ox} were generally low in the A and E horizons.

Most of the P in the B horizons was extracted by oxalate (≥64% of TP); the P_{ox} concentration ranged between 2.7 and 28.9 mmol kg^{-1}. The percentages decreased with soil depth for most of the soils. The lowest relative recovery of P_{ox} was found at Tärnsjö, particularly in the C horizon where P_{ox} formed, on average, 20% of TP. By contrast, the DPS was consistently the highest at Tärnsjö, exceeding 25% below 70 cm. The proportion of oxalate-extractable organic P ($P_{org\text{-}ox}$) in relation to P_{ox} was higher in the Oe and A/E horizons and then decreased with increasing soil depth and with decreasing organic C. Unlike P_{ox} and Pi_{ox}, $P_{org\text{-}ox}$ was strongly correlated with organic C ($r = 0.83$, $p < 0.001$).

3.3. P speciation in soils as evidenced by P K-edge XANES spectroscopy

The contribution of different P fractions varied within and among soil profiles (Figs. 2 and 3, Tables S2–S8). In the Oe horizons, $P_{org\text{-}lcf}$ was the dominant P fraction with a relative contribution between 73 (±3.5) and 91% (±2.4), but there was also a minor contribution from Al- and Fe-, and/or Ca-bound P. In the A/E horizons, the contribution of Al-bound P, $P_{org\text{-}lcf}$, Fe-bound P, and Ca-P were 16–68%, 17–57%, 0–43%, and 0–29%, respectively. Although $P_{org\text{-}lcf}$ and Ca-P were present in some of the B horizon samples, Al-bound P was the dominant P fraction in the B horizon. The Al-bound P consisted probably mostly of ITM, as evidenced both by the strong relationship between (Al_{ox}-Al_{py}) and Si_{ox} (Fig. S2), and by the fact that the "P adsorbed to allophane" standard occurred most frequently in the best fits (Tables S2–S8). Al-bound P contributed to 42–74% of TP followed by Fe-bound P with 5–24%. Of the Fe-bound P (P adsorbed to poorly crystalline Fe oxides + amorphous $FePO_4$), P adsorbed to ferrihydrite and goethite were the most abundant P species throughout the soil profiles, according to the LCF results (Tables S2–S8).

In all soils, Ca-bound P increased with increasing soil depth (Figs. 2 and 3). The Ca-bound P was probably dominated by apatite, which is supported by the fact that apatite occurred most frequently in the best LCF fits (Tables S2–S8). With the exception of the Kloten soil, which was underlain by bedrock at 50 cm, the content of Ca-bound P was 17–63 % in the C horizon down to 80 cm depth (Fig. 3). In the shallow Kloten soil, apatite appeared to have almost completely dissolved. By contrast, Tärnsjö appeared to be the soil with the highest amount of apatite in the C horizon, as Ca-bound P accounted for 63% of the TP between 40 and 80 cm depth (Fig. 2, Table S4). Al- and Fe-bound P were also common P species in the C horizon whereas the contribution of organic P was low, only 0–6%. It is also pertinent to note that there was general consistency between XANES and XRPD in the determination of apatite content within and between soils.

When taking into account bulk densities (Table S1), sample thickness, and stones and boulder content, the P stock in the upper 80 cm of the soils investigated ranged from 69.1 to 379.0 g P m^{-2}. It should be noted that the smallest P stock was calculated for Kloten, simply because its profile was shallower than the others. Unlike the higher P concentration in the surface horizons, the average stock of TP was only 4 g m^{-2} in the O horizons and 9.5 g m^{-2} in the A/E horizons, as compared to 117.5 g m^{-2} and 109.3 g m^{-2} in B and C (down to 80 cm), respectively, which means that 94 % of TP was in the B and C horizons. This substantially larger TP stock in the subsoil was caused in part by higher bulk densities (Table S1), thicker horizons but also by P redistribution. The stocks of separate P species in different horizons followed the same pattern as TP, i.e. high concentrations but low stocks in the O horizons and maximum P species stocks in the subsoil (Fig. 2). Of the TP in the subsoil, 58% was adsorbed P (mainly to Al), while apatite accounted for 25% of the P, most of which was in the C horizons. The apatite stocks in the A/E, B, and C horizons (down to 80 cm) was on average 2.5%, 20%, and 77.2% of the total apatite, respectively. It should be noted that the stocks in the E horizon of the Tärnsjö pedon were not calculated because of its low P concentration, which prevented successful XANES speciation. Moreover, the Asa O horizon was not available and therefore not included in the evaluation.

Possible relationships between XANES-derived P species and extraction results were investigated using correlation analysis. Notably, there was a significant positive correlation between the Ca-bound P, as evidenced by XANES-LCF, and DPS ($r = 0.57$, $p < 0.001$) across all 73 soil samples (Table 3), which suggests that a high apatite content led to higher dissolved P and thus to a higher degree of saturation on the Fe oxides and ITM. The $P_{org\text{-}lcf}$ was strongly correlated ($r = 0.91$, $p < 0.001$) with C_{org} and weakly but significantly correlated also with $P_{org\text{-}ox}$ ($r = 0.35$, $p < 0.05$). XANES-derived Fe- and Al-bound P was highly significantly correlated with total P_{ox} ($r = 0.97$, $p < 0.001$) as well as with P_{iox} ($r = 0.95$, $p < 0.001$). Moreover, a regression analysis showed that the determination coefficient was ($r^2 = 0.95$, $p < 0.001$), ($r^2 = 0.92$, $p < 0.001$), and (0.52, $p < 0.001$) for the pairs [XANES-(Fe + Al)-P; P_{ox}], [XANES-(Fe + Al)-P; Pi_{ox}], and [$P_{org\text{-}lcf}$; $P_{org\text{-}ox}$], respectively (Figs. 4

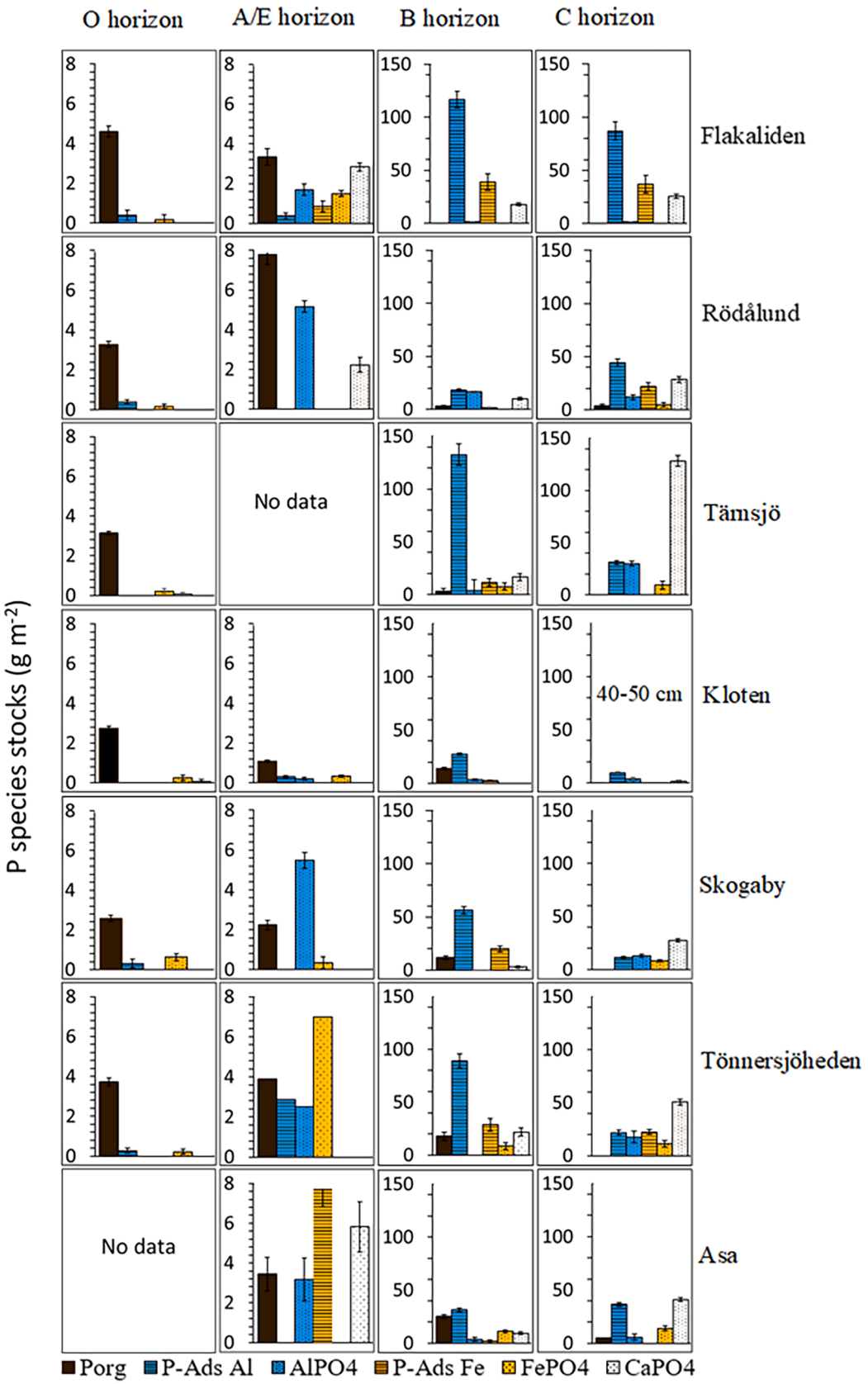

Fig. 2. Stocks of phosphorus (P) species groups in the organic layer, A/E, B, and C horizons (down to 80 cm) in seven forest soils from Sweden. No available data for O horizon for Asa, the E horizon for Tärnsjö, and below 50 cm for Kloten. Error bars indicate the uncertainty associated with the P pools.

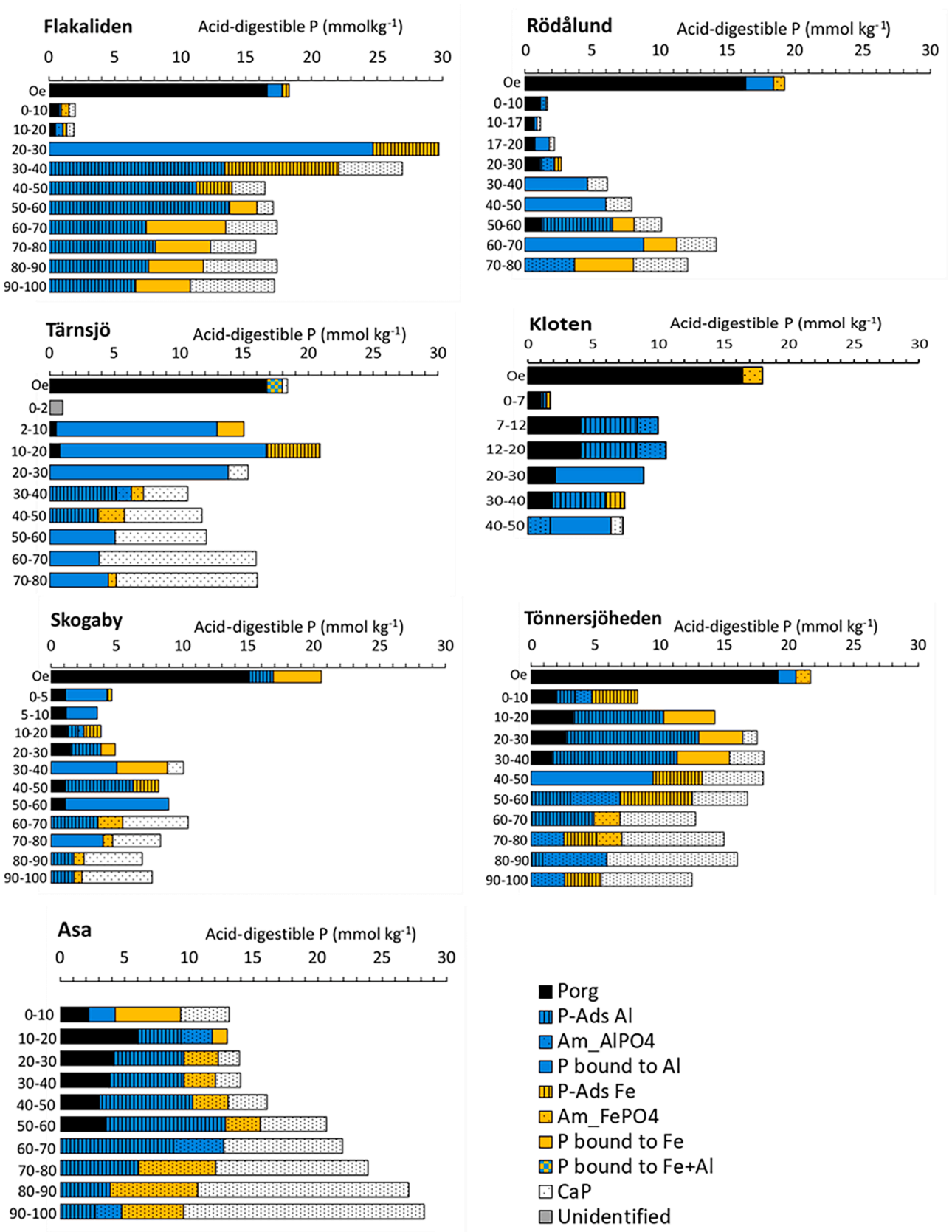

Fig. 3. Relative contributions of different P species to TP in seven forest soils according to P *K*-edge XANES spectroscopy. Soil depth (cm) is shown on the left. P_{org}: organic P, P bound to Al: the sum of all Al-bound P species, P bound to Fe: the sum of all Fe-bound P species. In the O horizon of Tärnsjö, P bound to Fe + Al represents a case when the probabilistic LCF could not differentiate between P bound to Al from P bound to Fe.

Table 3
Pearson correlation coefficients (r) between extractable P fractions, XANES-derived P species and selected soil properties across all investigated mineral soil horizons. ***: P < 0.001, **: P < 0.01,*: P < 0.05.

	pH	Al_{py}	Fe_{py}	Al_{ox}	Fe_{ox}	Si_{ox}	P_{ox}	Pi_{ox}	$P_{org\text{-}ox}$	C	DPS
TP	0.37**	0.17	0.00	0.28**	0.21	0.28*	0.84***	0.84***	0.26*	–0.07	0.41**
P_{ox}	0.01	0.31*	0.13	0.45***	0.40***	0.42***	–	0.97***	0.46**	0.1	0.08
Pi_{ox}	0.14	0.13	–0.05	0.35**	0.27*	0.39**	0.97***	–	0.23	–0.11	0.21
$P_{org\text{-}ox}$	–0.46***	0.78***	0.72***	0.53***	0.62***	0.25*	0.46***	0.23	–	0.83***	–0.46***
PAL	−0.02	−0.09	−0.05	−0.21	−0.15	−0.25*	0.43***	0.46***	–	−0.03	0.43***
P_{Ols}	−0.14	0.01	0.06	0	0.12	−0.05	0.65***	0.66***	–	0.12	0.30*
$P_{org\text{-}lcf}$	−0.24	−0.02	−0.01	−0.02	−0.03	−0.04	0.10	−0.02	0.35*	0.91***	0.3
(Fe + Al)-P	0.16	0.20	0.04	0.36**	0.32**	0.36**	0.97***	0.96***	0.33**	−0.20	0.22
Al-bound P	−0.19	0.17	0.03	0.32*	0.27*	0.31*	0.87***	0.87***	0.25*	−0.05	0.26*
Fe-bound P	0.23	0.25	0.03	0.54***	0.44**	0.54***	0.76***	0.76***	0.2	−0.13	0.04
P-ads Al	0.21	0.05	−0.08	0.24	0.18	0.19	0.87***	0.88***	0.18	−0.11	0.30*
$AlPO_4$	0.46*	−0.04	−0.17	0.02	−0.13	0.12	0.34	0.40*	0.00	−0.16	0.55**
P-ads Fe	0.34	0.37	0.04	0.55**	0.43*	0.51**	0.72***	0.71***	0.31	−0.04	0.17
$FePO_4$	0.05	0.12	0.00	0.25	0.13	0.38	0.80***	0.89***	0.05	−0.15	−0.08
$CaPO_4$	0.37*	−0.21	−0.22	−0.24	−0.22	−0.17	0.04	0.11	–0.22	−0.28	0.57***

and 5). Overall, these results suggest a high level of consistency between the XANES-derived P speciation results and the information gained from wet chemical extractions.

4. Discussion

The P speciation results of this study are consistent with those of Wood et al., who already in 1984 observed that the Podzols they studied were "highly stratified with respect to phosphorus biogeochemistry", with biological control of P in the O and some of the E horizons (as manifested in the predominance of organic P), while in the B horizons P cycling was predominantly "geochemical" and governed by P adsorption/desorption to secondary Al and Fe phases. They are also in general agreement with the Walker and Syers model (Walker and Syers, 1976), i.e., with time, primary mineral apatite is weathered to other P forms such as adsorbed P and organic P. Similar observations were also made by, e.g. Cade-Menun et al. (2000) and SanClements et al. (2010). These and other previous research findings were, however, based on traditional wet-chemistry fractionation methods and in some cases ^{31}P NMR spectroscopy, none of which are well suited to characterize inorganic P phases in subsoils. In the current study, the use of P *K*-edge XANES spectroscopy combined with traditional wet-chemistry methods permitted a more detailed picture of P speciation. Although similar work

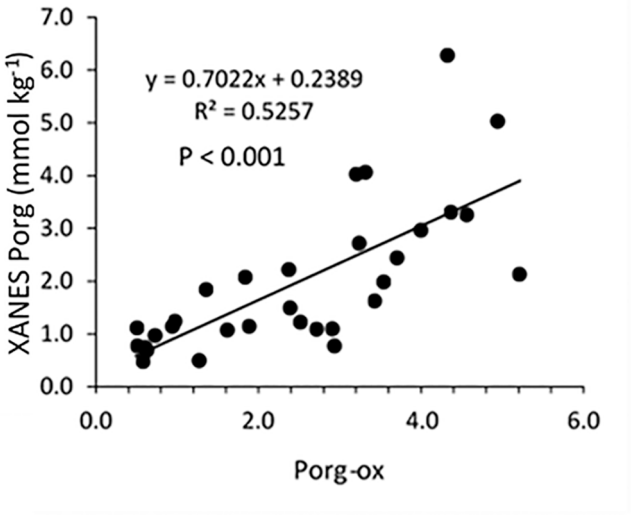

Fig. 5. Relationship between organic P (according to XANES) and organic P determined by oxalate extraction in the mineral soils.

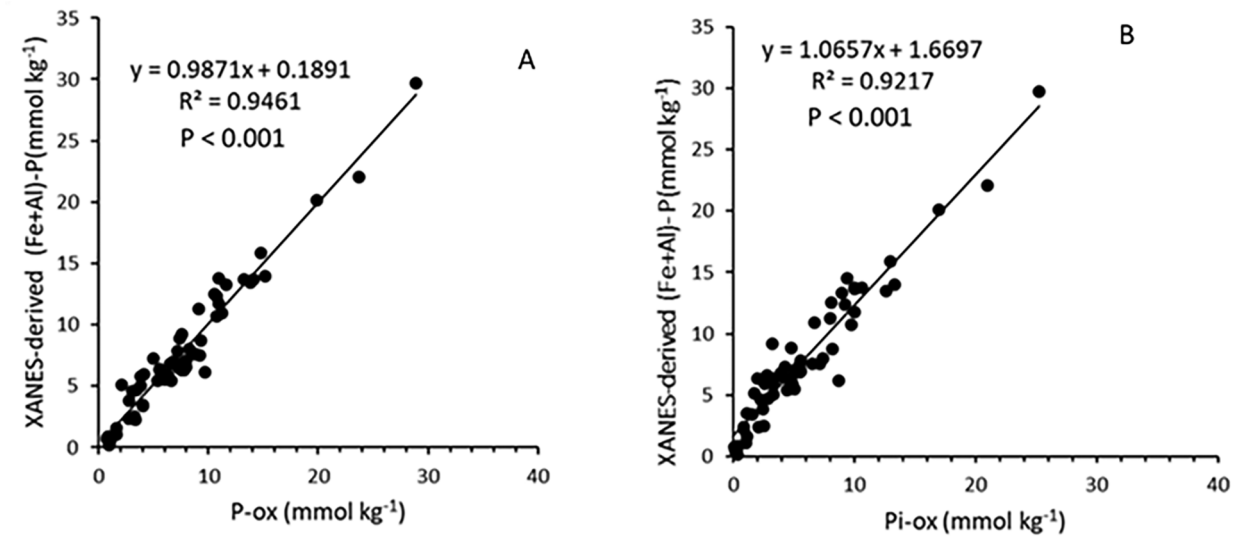

Fig. 4. Relationship of Fe- and Al-bound P (according to XANES) and (A) oxalate-extractable total P and (B) inorganic P, in all the 65 mineral soil samples from seven different forest soils.

was reported recently for other soil profiles from Cambisols and from other non-podzolized soils (Prietzel et al., 2016; Rodionov et al., 2020; Zhang et al., 2021), this study, together with a companion study (Adediran et al., 2020) are the first, to our knowledge, that report detailed XANES-derived P speciation data for Podzols and Podzol-like soils typical of boreal forested environments.

A unique aspect of the current study was the estimation of horizon-specific P stocks associated with different P species, as determined by XANES. These calculations show that in the seven studied profiles only a small part of the P resided in the O and E horizons (6%) while the remaining 94 % was found in the B and C horizons down to 80 cm. In line with this is the finding that, on average, only 6% of the P was organic P, while 58 % was adsorbed to Al and Fe (hydr)oxides (mainly to Al) and 25 % was Ca phosphates in the subsoil horizons. Thus, although the quantitative role of Al and Fe (hydr)oxide-bound P for P uptake has been questioned, it is nevertheless clear that this pool, together with apatite, represents a large reserve of P in the forest ecosystem. The P stocks of this study are in the low to intermediate range when compared to central European forest soils (Cambisols; Prietzel et al., 2016; Lang et al., 2017), and soils from the tropical East Asian region (Jien et al., 2016). The distribution of P species in podzolized soils of temperate regions has been also studied (Werner et al., 2017), although in this case stocks were not calculated.

The investigated forest soils show a marked decline in apatite contents (both in concentrations and stocks) in the topsoils down to about 30–40 cm depth compared to the C horizon after 10,000 to 15,000 years of soil formation. A large part of the TP has been transformed into organic P in the topsoils and to Fe- and Al-bound P in the B horizon. As concerns the B horizons, the XANES data allowed us to clarify the identity of the adsorbed P. Perhaps not surprisingly, P bound to Al and Fe (hydr)oxides and ITM were the major P forms. However, it should be noted that the ITM were of particular importance as a host for adsorbed P: as can be seen in Fig. 3 and Tables S2–S8, P adsorbed to allophane, and other Al-bound P forms, were quantitatively more important than Fe-bound P in all studied soils. There was also a strong increase in the apatite fraction in the mineral soil as a function of soil depth, which is also evident in the mineralogical analysis of soil by XRPD (Table S9). These results extend those of our previous study (Adediran et al., 2020), which used micro-focused X-ray fluorescence and absorption microscopy showing the subsoil apatite to occur both as inclusions in aluminosilicate minerals and as discrete mineral grains. These findings support the ideas of Wood et al. (1984), who found indications that surface horizons rich in roots, bacteria, fungi, and OM are layers of strict biological P retention whereas geochemical processes involving mostly inorganic P pools would predominate in underlying soil horizons. This is probably true for the Oe horizons of the current study, where organic C was about 40 %, and where organic P accounts for a major part of the TP. Previous research has shown that P cycling in forested ecosystems is characterized by tight coupling between the decomposition/mineralization of organic P and uptake in the surface horizon, so that only a minor fraction of the P is taken up from the subsoil (e.g. Klotzbücher et al., 2020; Lang et al., 2017; Wood et al., 1984).

Organic P decreased substantially with increasing soil depth and was a minor P species in the subsoil. The reason for this is likely that plant litter is the main source of P_{org} which is deposited on top of the organic layer (leaf litter) or mostly in the organic layer (root litter). In the mineral soil, organic matter is mainly derived from root litter and mycorrhizal fungi (Buurman and Jongmans, 2005, Richardson and Simpson, 2011) and their density decreases with soil depth, resulting in lower OM input thus low P_{org} (Wood et al., 1984). Alternatively, the occurrence of P_{org} in the subsoil might also be explained by leaching of DOC or colloids through the soil profile (e.g., Werner et al., 2017).

The C_{org}: P_{org} and N: P_{org} ratios in the A/E horizons were most often of a similar magnitude as in the Oe horizon (Table 2, and S1), but then decreased with increasing soil depth and with increasing P concentrations in the mineral soil. This agrees with previous research showing that high contents of surface Al and Fe minerals result in narrow C_{org}:P_{org} ratios (Werner et al., 2017). In the B horizons, most of the P was associated with Al and Fe phases, which reflects the enrichment of ITM and Fe (hydr)oxides in the B horizon due to podzolization processes (e.g. Lundström et al., 2000). Our results suggest that during pedogenesis, P weathered from apatite in the upper soil horizons has been redistributed, and a major part of this P is now adsorbed in the B horizon. A large part of this redistribution probably occurred early during the Holocene, as the apatite weathering rate was probably higher then (Zhou et al. 2018). The XANES results suggest that ITM was the most important host for adsorbed P in the B horizon. The mineralogical data of the soils studied support this interpretation as they show that allophane (ITM) and ferrihydrite peaked in B horizons (Table S9). The finding that ITM is the most important host for adsorbed P is not surprising given that (i) oxalate-extractable Al was generally much higher than oxalate-extractable Fe in the B horizon (Table 2), and (ii) surfaces with Al-OH groups have a documented high capacity to sorb orthophosphate (e.g. Tiberg et al. 2020). This finding is consistent with that of Takamoto et al. (2021) who found that Al phases exert a stronger control of P than Fe phases in allophanic soils.

The fact that 95% of the variation of the Fe- and Al-bound P could be explained by P_{ox} (which includes also organically bound P), compared to 92% for Pi_{ox} (Fig. 4), may suggest that organic P should not be ignored as a contributor to the Fe- and Al-bound P pool especially in the podzolized B horizons. As discussed by Gustafsson et al. (2020), adsorbed organic P may contribute to the XANES-derived Fe- and Al-bound P pool, as its XANES spectrum is intermediate to the spectra of adsorbed inorganic P and non-adsorbed organic P. These results are consistent with earlier studies (Borggaard et al., 2004, Yuan and Lavkulich, 1994), reporting that Fe and Al oxy(hydr)oxides are important sorbents for both mineral and organic P, especially in Podzols. To what extent the adsorbed P in the B horizon is available for uptake is a matter of ongoing discussion (Jones and Oburger, 2011; Klotzbücher et al. 2020). Excretion of organic acids from soil microorganisms can mobilize P in acid forest soils with limited P supply (Jones and Oburger, 2011). However, the P uptake by beech was not affected by addition of P-amended goethite in greenhouse experiments (Klotzbücher et al. 2020), which led these authors to put into question the ecological relevance of the large Fe-bound P pool in the subsoil.

In this context, it may be important to consider the fact that ITM and Fe oxide in the B horizon have high P sorption capacities and may serve not only as sources but also as sinks of P. To what extent they can act as sources is probably dependent on the DPS, i.e. to what extent the oxide surfaces are ‘saturated’ with P. Excretion of organic acids may not lead to increased P uptake if the released P is immediately readsorbed to the Fe and Al phases because of their low DPS. It is of interest to note that the Kloten soil, which was the soil with the lowest DPS in the B horizon, was also the soil with the largest percentage of P as organic P in the B horizon, despite its relatively strong accumulation of ITM and Fe oxide (Fig. 3, Table 2) as shown by extraction (Fig. S1 and S1) and XRPD results (Table S9). Conversely in the Tärnsjö soil, which had the highest DPS in the B horizon, the mineral soil contained very little organic P. This supports the idea that in relatively P-poor Podzols the system would strive for more efficient recycling of organic P, with minimal losses to adsorbed P forms in the subsoil (e.g. Lang et al., 2017; Odum, 2014).

Although the current study confirms the hypothesis of Wood et al. (1984), i.e. that Fe and Al in the subsoil exert a major control of P through geochemical rather than biological cycling, this does not exclude a role of Fe- and Al-bound P for biological uptake, particularly not in P-rich sites. In this respect we hypothesize that ITM and other Al phases such as $Al(OH)_3$, which dominate the P speciation in the B horizon of these boreal Podzols, are more likely sources for geochemically active P than Fe oxides, because of their lower thermodynamic stability under acid conditions (Gustafsson, 2001, Gypser et al., 2021).

In the C horizon, the apatite pool was larger in most of the studied soils, especially in Tärnsjö, Tönnersjöheden, and Flakaliden, which also

have relatively large P stocks. In addition, the DPS in the B and C horizons of these three soils was on average above 8% and 14%, respectively. This suggests that apatite weathering is still going on, which is supported by the fact that the pH is sufficiently low for apatite to be unstable. The result of acid P-AL (pH 3.75) (Table 2, S1) may also indicate that more P is dissolved at low pH in the apatite-dominated C horizon compared with the B horizon, in which Fe and Al are the major P hosts. In the Kloten soil, however, where the DPS was lowest, apatite had been almost completely dissolved from the pedon (Figs. 2 and 3). These trends demonstrate that the long-term effect of apatite weathering on the P availability in these boreal forest soils is substantial, and indicate that apatite-bound P represents a pool that is potentially available via deep root uptake.

5. Conclusions

- In the studied soils, 94% of the TP resides in the mineral soil from about 20 cm to 80 cm depth as adsorbed P and apatite. Although the mobilization of P from secondary Fe and Al compounds has been questioned, this study suggests that these pools could be P resources on which plants can rely in the long term for P uptake, especially since the P stocks in the surface horizons and topsoils soils are small.
- The combined use of bulk P *K*-edge XANES spectroscopy and wet-chemical P extractions revealed that organic P dominated the speciation in the organic horizon, whereas PO_4 bound to Fe and Al (hydr)oxides predominated in the B horizon of the studied soils. Al-bound P was higher than Fe-bound P, which may partly reflect the higher content of Al (hydr)oxides including ITM in the B horizon when compared to Fe (hydr)oxides.
- Apatite has been strongly weathered in the topsoils down to about 30–40 cm although the Swedish forest soils are at an early stage of soil development. As a result of podzolization, P from the topsoils (A/E horizons) has been redistributed to the B horizons, most probably as P adsorbed to ITM.
- The degree of P saturation (DPS) varied among the soils and was positively correlated with the content of Ca-bound P, which suggests that apatite weathering remains a determinant of long-term P availability in these soils.

Declaration of Competing Interest

The authors declare that they have no known competing financial interests or personal relationships that could have appeared to influence the work reported in this paper.

Acknowledgements

The work was funded by the Swedish Research Council Formas, grant number 2017-01139, by the Geological Survey of Sweden, grant number 36-2044-2016, and by the Swedish Farmers' Foundation for Agricultural Research, grant number O-15-23-311. We acknowledge the technical support of the staff at the BL8 at the Synchrotron Light Research Institute, Thailand. We also thank Mina Spångberg, Agnieszka Renman for their support during the P analysis.

Appendix A. Supplementary data

Supplementary data to this article can be found online at https://doi.org/10.1016/j.geoderma.2021.115500.

References

Adediran, G.A., Tuyishime, J.M., Vantelon, D., Klysubun, W., Gustafsson, J.P., 2020. Phosphorus in 2D: spatially resolved P speciation in two Swedish forest soils as influenced by apatite weathering and podzolization. Geoderma 376, 114550.

Akselsson, C., Westling, O., Alveteg, M., Thelin, G., Fransson, A.-M., Hellsten, S., 2008. The influence of N load and harvest intensity on the risk of P limitation in Swedish forest soils. Sci. Total Environ. 404, 284–289.

Albaugh, T.J., Bergh, J., Lundmark, T., Nilsson, U., Stape, J.L., Allen, H.L., Linder, S., 2009. Do biological expansion factors adequately estimate stand-scale aboveground component biomass for Norway spruce? For. Ecol. Manage. 258, 2628–2637.

Andersson, M., Carlsson, M., Ladenberger, A., Morris, G., Sadeghi, M., Uhlbäck, J., 2014. Geochemical atlas of Sweden (Geokemisk atlas över Sverige). Sveriges geologiska undersökning.

Beauchemin, S., Hesterberg, D., Chou, J., Beauchemin, M., Simard, R.R., Sayers, D.E., 2003. Speciation of phosphorus in phosphorus-enriched agricultural soils using X-ray absorption near-edge structure spectroscopy and chemical fractionation. J. Environ. Qual. 32, 1809–1819.

Bergh, J., Linder, S., Lundmark, T., Elfving, B., 1999. The effect of water and nutrient availability on the productivity of Norway spruce in northern and southern Sweden. For. Ecol. Manage. 119, 51–62.

Blakemore, L., 1987. Soil Bureau Laboratory Methods. A. Methods for chemical analysis of soils. NZ Soil Bureau Sci. Rep. 80, 44–45.

Borggaard, O.K., Szilas, C., Gimsing, A.L., Rasmussen, L.H., 2004. Estimation of soil phosphate adsorption capacity by means of a pedotransfer function. Geoderma 118, 55–61.

Buendia, C., Kleidon, A., Porporato, A., 2010. The role of tectonic uplift, climate, and vegetation in the long-term terrestrial phosphorous cycle. Biogeosciences 7, 2025–2038.

Butler, B.M., Hillier, S., 2021. Automated full-pattern summation of X-ray powder diffraction data for high-throughput quantification of clay-bearing mixtures. Clays Clay Miner. 69, 38–51.

Buurman, P., Jongmans, A., 2005. Podzolisation and soil organic matter dynamics. Geoderma 125, 71–83.

Buurman, P., Van Reeuwijk, L., 1984. Proto-imogolite and the process of podzol formation: a critical note. J. Soil Sci. 35, 447–452.

Cade-Menun, B.J., Berch, S.M., Preston, C.M., Lavkulich, L.M., 2000. Phosphorus forms and related chemistry of Podzolic soils on northern Vancouver Island. I. A comparison of two forest types. Can. J. For. Res. 30, 1714–1725.

Casetou-Gustafson, S., Akselsson, C., Hillier, S., Olsson, B.A., 2019. The importance of mineral determinations to PROFILE base cation weathering release rates: a case study. Biogeosciences 16, 1903–1920.

Casetou-Gustafson, S., Grip, H., Hillier, S., Linder, S., Olsson, B.A., Simonsson, M., Stendahl, J., 2020. Current, steady-state and historical weathering rates of base cations at two forest sites in northern and southern Sweden: a comparison of three methods. Biogeosciences 17, 281–304.

Casetou-Gustafson, S., Hillier, S., Akselsson, C., Simonsson, M., Stendahl, J., Olsson, B.A., 2018. Comparison of measured (XRPD) and modeled (A2M) soil mineralogies: a study of some Swedish forest soils in the context of weathering rate predictions. Geoderma 310, 77–88.

Chadwick, O.A., Derry, L.A., Vitousek, P.M., Huebert, B.J., Hedin, L.O., 1999. Changing sources of nutrients during four million years of ecosystem development. Nature 397, 491–497.

Church, C., Spargo, J., Fishel, S., 2017. Strong acid extraction methods for "total phosphorus" in soils: EPA Method 3050B and EPA Method 3051. Agric. Environ. Lett. 2, 160037.

Colocho Hurtarte, L.C., Souza-filho, L.F., Oliveira Santos, W., Vergütz, L., Prietzel, J., Hesterberg, D., 2019. Optimization of data processing minimizes impact of self-absorption on phosphorus speciation results by P K-edge XANES. Soil Syst. 3, 61.

Egnér, H., Riehm, H., Domingo, W., 1960. Untersuchungen über die chemische Bodenanalyse als Grundlage für die Beurteilung des Nährstoffzustandes der Böden. II. *Chemische Extraktionsmethoden zur Phosphor-und Kaliumbestimmung*. Kungliga Lantbrukshögskolans Annaler 26, 199–215.

Elser, J.J., Bracken, M.E., Cleland, E.E., Gruner, D.S., Harpole, W.S., Hillebrand, H., Ngai, J.T., Seabloom, E.W., Shurin, J.B., Smith, J.E., 2007. Global analysis of nitrogen and phosphorus limitation of primary producers in freshwater, marine and terrestrial ecosystems. Ecol. Lett. 10, 1135–1142.

Eriksson, A.K., Hesterberg, D., Klysubun, W., Gustafsson, J.P., 2016a. Phosphorus dynamics in Swedish agricultural soils as influenced by fertilization and mineralogical properties: Insights gained from batch experiments and XANES spectroscopy. Sci. Total Environ. 566, 1410–1419.

Eriksson, A.K., Hillier, S., Hesterberg, D., Klysubun, W., Ulén, B., Gustafsson, J.P., 2016b. Evolution of phosphorus speciation with depth in an agricultural soil profile. Geoderma 280, 29–37.

Franke, R., Hormes, J., 1995. The P K-near edge absorption spectra of phosphates. Physica B 216, 85–95.

Giesler, R., Petersson, T., Högberg, P., 2002. Phosphorus limitation in boreal forests: effects of aluminum and iron accumulation in the humus layer. Ecosystems 5, 300–314.

Gustafsson, J., Bhattacharya, P., Bain, D., Fraser, A., Mchardy, W., 1995. Podzolisation mechanisms and the synthesis of imogolite in northern Scandinavia. Geoderma 66, 167–184.

Gustafsson, J.P., Bhattacharya, P., Karltun, E., 1999. Mineralogy of poorly crystalline aluminium phases in the B horizon of Podzols in southern Sweden. Appl. Geochem. 14, 707–718.

Gustafsson, J.P., 2001. Modelling competitive anion adsorption on oxide minerals and an allophane-containing soil. Eur. J. Soil Sci. 52, 639–653.

Gustafsson, J.P., Braun, S., Tuyishime, J., Adediran, G.A., Warrinnier, R., Hesterberg, D., 2020. A probabilistic approach to phosphorus speciation of soils using P K-edge XANES spectroscopy with linear combination fitting. Soil Systems 4, 26.

Gypser, S., Schütze, E., Freese, D., 2021. Single and binary Fe-and Al-hydroxides affect potential phosphorus mobilization and transfer from pools of different availability. Soil Systems 5, 33.
Hesterberg, D., 2019. Response to letter to the editor on synchrotron-based identification of reaction products in phosphorus fertilized alkaline soils. Geofis. Int. 337, 150–151.
Hesterberg, D., 2010. Macroscale chemical properties and X-ray absorption spectroscopy of soil phosphorus. Developments in Soil Science. Elsevier.
Hesterberg, D., Zhou, W., Hutchison, K., Beauchemin, S., Sayers, D., 1999. XAFS study of adsorbed and mineral forms of phosphate. J. Synchrotron Radiat. 6, 636–638.
Heuck, C., Smolka, G., Whalen, E.D., Frey, S., Gundersen, P., Moldan, F., Fernandez, I.J., Spohn, M., 2018. Effects of long-term nitrogen addition on phosphorus cycling in organic soil horizons of temperate forests. Biogeochemistry 141, 167–181.
Hewitt, A.E., Balks, M.R., Lowe, D.J., 2021. Allophanic Soils. The Soils of Aotearoa New Zealand. Springer International Publishing, Cham.
Hillier, S., 1999. Use of an air brush to spray dry samples for X-ray powder diffraction. Clay Miner. 34, 127–135.
Ilg, K., Wellbrock, N., Lux, W., 2009. Phosphorus supply and cycling at long-term forest monitoring sites in Germany. Eur. J. Forest Res. 128, 483–492.
Iso, D., 1998. 13878. Soil quality-Determination of total nitrogen content by dry combustion (“ elemental analysis”)(ISO 13878: 1998),“ vol., no.
IUSS Working Group WRB. 2014. World reference base for soil resources 2014. International soil classification system for naming soils and creating legends for soil maps. World Soil Resources Reports No. 106. FAO, Rome.
Jien, S.-H., Baillie, I., Hu, C.-C., Chen, T.-H., Iizuka, Y., Chiu, C.-Y., 2016. Forms and distribution of phosphorus in a placic podzolic toposequence in a subtropical subalpine forest, Taiwan. Catena 140, 145–154.
Jonard, M., Fürst, A., Verstraeten, A., Thimonier, A., Timmermann, V., Potočić, N., Waldner, P., Benham, S., Hansen, K., Merilä, P., 2015. Tree mineral nutrition is deteriorating in Europe. Glob. Change Biol. 21, 418–430.
Jones, D.L., Oburger, E., 2011. Solubilization of phosphorus by soil microorganisms. Phosphorus in Action. Springer.
Karltun, E., Bain, D.C., Gustafsson, J.P., Mannerkoski, H., Murad, E., Wagner, U., Fraser, A.R., Mchardy, W.J., Starr, M., 2000. Surface reactivity of poorly-ordered minerals in podzol B horizons. Geoderma 94, 265–288.
Kelly, S., Hesterberg, D., Ravel, B., 2008. Analysis of soils and minerals using X-ray absorption spectroscopy. Methods Soil Anal. Part 5 5, 387–463.
Klotzbücher, A., Schunck, F., Klotzbücher, T., Kaiser, K., Glaser, B., Spohn, M., Widdig, M., Mikutta, R., 2020. Goethite-associated phosphorus is not available to beech (Fagus sylvatica L.). Front. Forests Global Change 3, 94.
Klysubun, W., Tarawarakarn, P., Thamsanong, N., Amonpattaratkit, P., Cholsuk, C., Lapboonrueng, S., Chaichuay, S., Wongtepa, W., 2020. Upgrade of SLRI BL8 beamline for XAFS spectroscopy in a photon energy range of 1–13 keV. Radiat. Phys. Chem. 175, 108145.
Lang, F., Bauhus, J., Frossard, E., George, E., Kaiser, K., Kaupenjohann, M., Krüger, J., Matzner, E., Polle, A., Prietzel, J., 2016. Phosphorus in forest ecosystems: new insights from an ecosystem nutrition perspective. J. Plant Nutr. Soil Sci. 179, 129–135.
Lang, F., Krüger, J., Amelung, W., Willbold, S., Frossard, E., Bünemann, E.K., Bauhus, J., Nitschke, R., Kandeler, E., Marhan, S., 2017. Soil phosphorus supply controls P nutrition strategies of beech forest ecosystems in Central Europe. Biogeochemistry 136, 5–29.
Lim, H., Olsson, B.A., Lundmark, T., Dahl, J., Nordin, A., 2020. Effects of whole-tree harvesting at thinning and subsequent compensatory nutrient additions on carbon sequestration and soil acidification in a boreal forest. GCB Bioenergy 12, 992–1001.
Linder, S., 1995. Foliar analysis for detecting and correcting nutrient imbalances in Norway spruce. Ecol. Bull. 178–190.
Lundström, U.V., Van Breemen, N., Bain, D., Van Hees, P., Giesler, R., Gustafsson, J.P., Ilvesniemi, H., Karltun, E., Melkerud, P.-A., Olsson, M., 2000. Advances in understanding the podzolization process resulting from a multidisciplinary study of three coniferous forest soils in the Nordic Countries. Geoderma 94, 335–353.
Mehmood, A., Akhtar, M.S., Imran, M., Rukh, S., 2018. Soil apatite loss rate across different parent materials. Geoderma 310, 218–229.
Mohren, G., Van Den Burg, J., Burger, F., 1986. Phosphorus deficiency induced by nitrogen input in Douglas fir in the Netherlands. Plant Soil 95, 191–200.
Nezat, C.A., Blum, J.D., Yanai, R.D., Hamburg, S.P., 2007. A sequential extraction to determine the distribution of apatite in granitoid soil mineral pools with application to weathering at the Hubbard Brook Experimental Forest, NH, USA. Appl. Geochem. 22, 2406–2421.
Nezat, C.A., Blum, J.D., Yanai, R.D., Park, B.B., 2008. Mineral sources of calcium and phosphorus in soils of the northeastern United States. Soil Sci. Soc. Am. J. 72, 1786–1794.
Nilsson, T., Lundin, L., 2006. Prediction of bulk density in Swedish forest soils from the organic carbon content and soil depth. Rep. For. Ecol. For. Soils 91, 41.
Odum, E.P., 2014. The strategy of ecosystem development. The Ecological Design and Planning Reader. Springer.
Olsen, S.R., 1954. Estimation of available phosphorus in soils by extraction with sodium bicarbonate, US Department of Agriculture.
Omotoso, O., McCarty, D.K., Hillier, S., Kleeberg, R., 2006. Some successful approaches to quantitative mineral analysis as revealed by the 3rd Reynolds Cup contest. Clays Clay Miner. 54, 748–760.
Porder, S., Hilley, G.E., 2011. Linking chronosequences with the rest of the world: predicting soil phosphorus content in denuding landscapes. Biogeochemistry 102, 153–166.
Prietzel, J., Dümig, A., Wu, Y., Zhou, J., Klysubun, W., 2013. Synchrotron-based P K-edge XANES spectroscopy reveals rapid changes of phosphorus speciation in the topsoil of two glacier foreland chronosequences. Geochim. Cosmochim. Acta 108, 154–171.
Prietzel, J., Klysubun, W., Werner, F., 2016. Speciation of phosphorus in temperate zone forest soils as assessed by combined wet-chemical fractionation and XANES spectroscopy. J. Plant Nutr. Soil Sci. 179, 168–185.
Ravel, B., 2009. ATHENA user’s guide. Athena IFFEFIT.
Ravel, B., Newville, M., 2005. ATHENA, ARTEMIS, HEPHAESTUS: data analysis for X-ray absorption spectroscopy using IFEFFIT. J. Synchrotron Radiat. 12, 537–541.
Richardson, A.E., Simpson, R.J., 2011. Soil microorganisms mediating phosphorus availability update on microbial phosphorus. Plant Physiol. 156, 989–996.
Rodionov, A., Bauke, S.L., von Sperber, C., Hoeschen, C., Kandeler, E., Kruse, J., Lewandowski, H., Marhan, S., Mueller, C.W., Simon, M., Tamburini, F., Uhlig, D., von Blanckenburg, F., Lang, F., Amelung, W., 2020. Biogeochemical cycling of phosphorus in subsoils of temperate forest ecosystems. Biogeochemistry 150, 313–328.
SanClements, M.D., Fernandez, I.J., Norton, S.A., 2010. Phosphorus in soils of temperate forests: linkages to acidity and aluminum. Soil Sci. Soc. Am. J. 74, 2175–2186.
Selmants, P.C., Hart, S.C., 2010. Phosphorus and soil development: does the Walker and Syers model apply to semiarid ecosystems? Ecology 91, 474–484.
Simonsson, M., Bergholm, J., Lemarchand, D., Hillier, S., 2016. Mineralogy and biogeochemistry of potassium in the Skogaby experimental forest, southwest Sweden: pools, fluxes and K/Rb ratios in soil and biomass. Biogeochemistry 131, 77–102.
Simonsson, M., Bergholm, J., Olsson, B.A., Von Brömssen, C., Öborn, I., 2015. Estimating weathering rates using base cation budgets in a Norway spruce stand on podzolised soil: analysis of fluxes and uncertainties. For. Ecol. Manage. 340, 135–152.
Smits, M.M., Johansson, L., Wallander, H., 2014. Soil fungi appear to have a retarding rather than a stimulating role on soil apatite weathering. Plant Soil 385, 217–228.
Stendahl, J., Akselsson, C., Melkerud, P.-A., Belyazid, S., 2013. Pedon-scale silicate weathering: comparison of the PROFILE model and the depletion method at 16 forest sites in Sweden. Geoderma 211, 65–74.
Stendahl, J., Lundin, L., Nilsson, T., 2009. The stone and boulder content of Swedish forest soils. Catena 77, 285–291.
Strand, L.T., Callesen, I., Dalsgaard, L., De Wit, H.A., 2016. Carbon and nitrogen stocks in Norwegian forest soils—the importance of soil formation, climate, and vegetation type for organic matter accumulation. Can. J. For. Res. 46, 1459–1473.
Takamoto, A., Hashimoto, Y., Asano, M., Noguchi, K., Wagai, R., 2021. Distribution and chemical species of phosphorus across density fractions in Andisols of contrasting mineralogy. Geoderma 395, 115080.
Talkner, U., Meiwes, K.J., Potočić, N., Seletković, I., Cools, N., De Vos, B., Rautio, P., 2015. Phosphorus nutrition of beech (Fagus sylvatica L.) is decreasing in Europe. Ann. Forest Sci. 72, 919–928.
Tiberg, C., Sjöstedt, C., Eriksson, A.K., Klysubun, W., Gustafsson, J.P., 2020. Phosphate competition with arsenate on poorly crystalline iron and aluminum (hydr) oxide mixtures. Chemosphere 255, 126937.
Tiberg, C., Sjöstedt, C., Gustafsson, J.P., 2018. Metal sorption to Spodosol Bs horizons: Organic matter complexes predominate. Chemosphere 196, 556–565.
Turner, B.L., Condron, L.M., 2013. Pedogenesis, Nutrient Dynamics, and Ecosystem Development: The Legacy of TW Walker and JK Syers. Springer.
Walker, T., Syers, J.K., 1976. The fate of phosphorus during pedogenesis. Geoderma 15, 1–19.
Van Reeuwijk, L. P., 1986. Procedures for soil analysis.
Werner, F., De La Haye, T.R., Spielvogel, S., Prietzel, J., 2017. Small-scale spatial distribution of phosphorus fractions in soils from silicate parent material with different degree of podzolization. Geoderma 302, 52–65.
Werner, F., Prietzel, J.R., 2015. Standard protocol and quality assessment of soil phosphorus speciation by PK-Edge XANES spectroscopy. Environ. Sci. Technol. 49, 10521–10528.
Vincent, A.G., Vestergren, J., Gröbner, G., Persson, P., Schleucher, J., Giesler, R., 2013. Soil organic phosphorus transformations in a boreal forest chronosequence. Plant Soil 367, 149–162.
Viro, P., 1952. Kivisyyden määrittämisestä. On the determination of stoniness. Commun. Instituti Forestalis Fenniae 40, 23.
Vitousek, P.M., Porder, S., Houlton, B.Z., Chadwick, O.A., 2010. Terrestrial phosphorus limitation: mechanisms, implications, and nitrogen–phosphorus interactions. Ecol. Appl. 20, 5–15.
Wolf, A., Baker, D., 1990. Colorimetric method for phosphorus measurement in ammonium oxalate soil extracts. Commun. Soil Sci. Plant Anal. 21, 2257–2263.
Wood, T., Bormann, F., Voigt, G., 1984. Phosphorus cycling in a northern hardwood forest: biological and chemical control. Science 223, 391–393.
Yanai, R.D., 1998. The effect of whole-tree harvest on phosphorus cycling in a northern hardwood forest. For. Ecol. Manage. 104, 281–295.
Yu, L., Zanchi, G., Akselsson, C., Wallander, H., Belyazid, S., 2018. Modeling the forest phosphorus nutrition in a southwestern Swedish forest site. Ecol. Model. 369, 88–100.
Yuan, G., Lavkulich, L., 1994. Phosphate sorption in relation to extractable iron and aluminum in Spodosols. Soil Sci. Soc. Am. J. 58, 343–346.

Zetterberg, T., Olsson, B.A., Löfgren, S., Von Brömssen, C., Brandtberg, P.-O., 2013. The effect of harvest intensity on long-term calcium dynamics in soil and soil solution at three coniferous sites in Sweden. For. Ecol. Manage. 302, 280–294.
Zhang, Z., Zhao, Z., Liu, C., Chadwick, O.A., Liang, C., Hu, Y., Vaughan, K., Zhu, M., 2021. Vertical patterns of phosphorus concentration and speciation in three forest soil profiles of contrasting climate. Geochim. Cosmochim. Acta 310, 1–18.
Zhou, J., Bing, H., Wu, Y., Sun, H., Wang, J., 2018. Weathering of primary mineral phosphate in the early stages of ecosystem development in the Hailuogou Glacier foreland chronosequence. Eur. J. Soil Sci. 69, 450–461.